




Article

Reactive Sintering of Cemented Carbides

Victor I. Stanciu ^{1,*} , Alexandre Mégret ¹ , Anne Mouftiez ², Véronique Vitry ¹  and Fabienne Delaunois ^{1,*}¹ Metallurgy Department, University of Mons, 7000 Mons, Belgium; alexandre.megret@umons.ac.be (A.M.); veronique.vitry@umons.ac.be (V.V.)² Institut Catholique d'Arts et Metiers, 59000 Lille, France; anne.mouftiez@icam.fr

* Correspondence: victorioan.stanciu@umons.ac.be (V.I.S.); fabienne.delaunois@umons.ac.be (F.D.)

Abstract

Cemented carbides are among the primary materials for tools and wear parts. Today, energy prices and carbon emissions have become key concerns worldwide. Cemented carbides consist of tungsten carbide combined with a binder, typically cobalt, nickel, or more recently, various high-entropy alloys. Producing tungsten carbide involves reducing tungsten oxide, followed by carburization of tungsten at 1400 °C under a hydrogen atmosphere. The tungsten carbide produced is then mixed with the binder, milled to achieve the desired particle size, and granulated to ensure proper flow for pressing and shaping. This study aims to bypass the tungsten carburizing step by mixing tungsten, carbon, and cobalt; shaping the mixture; and then applying reactive sintering, which will convert tungsten into carbide and consolidate the parts. The mixtures were prepared by planetary ball milling for 10 h under different conditions. Tests demonstrated that tungsten carburization successfully occurs during sintering at 1450 °C for 1 h. The samples exhibit a typical cemented carbide microstructure, characterized by prismatic grains with an average size of 0.32 µm. Densification reached 92%, hardness is approximately 1800 HV30, and toughness is $10.9 \pm 1.15 \text{ MPa}\cdot\text{m}^{1/2}$.

Keywords: cemented carbides; doped cobalt; reactive sintering

Academic Editors: Christopher C. Berndt and Andrew Ang

Received: 26 May 2025

Revised: 11 July 2025

Accepted: 22 July 2025

Published: 25 July 2025

Citation: Stanciu, V.I.; Mégret, A.; Mouftiez, A.; Vitry, V.; Delaunois, F. Reactive Sintering of Cemented Carbides. *Alloys* **2025**, *4*, 15. <https://doi.org/10.3390/alloys4030015>

Copyright: © 2025 by the authors. Licensee MDPI, Basel, Switzerland. This article is an open access article distributed under the terms and conditions of the Creative Commons Attribution (CC BY) license (<https://creativecommons.org/licenses/by/4.0/>).

1. Introduction

Tungsten carbide is a staple product of the cemented carbide industry. The conventional production of this material involves reducing tungsten oxides, carburizing tungsten, mixing it with cobalt, and then shaping and sintering [1].

Traditionally, tungsten carbide is manufactured by carburizing tungsten at a temperature of 1300–1400 °C under a hydrogen atmosphere; the size of the obtained powder depends on the size of the tungsten particles subjected to carburizing [2,3]. After the carburizing process, the resulting powder, which is somewhat agglomerated, requires grinding to reach the desired particle size distribution [4]. Carburization of tungsten can also occur at lower temperatures [5]. The presence of cobalt accelerates this process, as revealed in Wangbin Zhan's study [6].

Reactive sintering can bypass the carburization step [7]. Reactive sintering is a process in which particle consolidation and conversion reactions between the elementary components co-occur to form the main powder component.

Eliminating the carburizing process in the manufacturing route of hardmetals will be a step forward in enhancing the sustainability of these highly technological materials. Significant savings will result from avoiding the need to heat the powder at 1400 °C and

from not using a hydrogen atmosphere, an expensive gas (which is not yet very “green”) that requires additional safety precautions due to the risk of explosion [8].

Reactive sintering of WC-based cemented carbides is seldom documented in the literature [9]. A review of existing studies shows few references that use tungsten–carbon–cobalt mixtures followed by reactive sintering in traditional furnaces to produce wear-resistant parts. However, Sun et al. [10] successfully manufactured WC powders and compacts using spark plasma sintering (SPS). Reactive sintering with tungsten nitride as the tungsten source, without cobalt or other binders, highlights the difficulty of managing gas emissions during the reduction process of tungsten nitride. Therefore, using pure tungsten as a raw material for reactive sintering is more attractive, as it avoids gas emissions from carburization. A recent study [11] demonstrates that it is possible to produce Co-WC composites from a 10 h milled W-C-Co blend through vacuum sintering, even though the cobalt content, around 80 wt.%, makes it unsuitable for cutting tools.

This work will examine the feasibility of producing WC-Co composites with optimal properties (hardness of 1700–1900 HV and toughness of at least 10 MPa·m^{1/2}) from a mixture of elemental powders, followed by reactive sintering within the composition range (6–12 wt.% Co) used in the tool industry.

2. Experimental Section

The mixture used in this study consists of 90 wt.% tungsten and carbon in a stoichiometric proportion, to which 10% by weight of doped cobalt was added (described below).

Tungsten powder, provided by Goodfellow, with a purity of 99.9% and a particle size of 0.5 µm was used for the study, to which black carbon powder from Alpha Aesar (Ward Hill, MA, USA), with a particle size of less than 25 nm, was added. This carbon powder is almost amorphous, giving it greater reactivity. Cobalt powder was produced in a laboratory by grinding cobalt granules with a purity of 99.5% (the rest being iron and manganese). The fraction used has a particle size smaller than 90 µm [12]. This cobalt powder was mixed with 10% by weight of chromium carbide (Cr₃C₂) and milled for 10 h in ethanol, following the procedure described in our previous paper [12], to produce a doped binder powder with a *d*₅₀ of 22 µm. The presence of chromium carbide in the binder limits the solubility of tungsten carbide during sintering, acting as a grain growth inhibitor (GGI). The effectiveness of this GGI method was also confirmed recently by Sadangi et al. [13]. The mixture was homogenized by milling in a Fritsch Pulverizette 7 Premium Line planetary mill (Idar-Oberstein, Germany), equipped with two 80 mL capacity bowls. Two types of milling equipment were used: the first consisted of martensitic stainless-steel bowls and 100 g of martensitic stainless-steel balls that were 10 mm in diameter as the milling medium and the second consisted of two WC-6Co-lined bowls and 200 g of WC-Co balls that were 10 mm in diameter as the milling medium in each bowl. A ball/powder ratio of 4:1 was maintained in each milling series. The milling parameters are provided in Table 1.

Table 1. Milling parameters for powder preparation.

Milling Series	Milling Speed [rpm]	Milling Time [h]	Milling Environment	Milling Media
S1	600	10	20 mL of ethanol	Ø10 mm, steel
S2	600	10	20 mL of ethanol	Ø10 mm, WC-6Co

Four samples were prepared by dry pressing 3 g of powder in a 1 cm² die at 294 MPa for about 20 s.

Samples were sintered in a tubular furnace (ThermoConcept, Bremen, Germany) at 1450 °C for 1 h, with a heating rate of 4 °C/min. The sintering process was conducted under vacuum until 350 °C, where a 30 min isothermal hold was used to remove the pressing agent. Subsequently, a flux composed of 95% Ar and 5% H₂ was circulated at a flow rate of 10 L/h.

The samples' density was measured using the Archimedes method.

Sintered samples were embedded in resin and polished with a Struers hard materials polishing kit. The microstructure was revealed by etching with Murakami's metallurgical reagent. It was examined using optical microscopy (Hirox KH-8700, Tokyo, Japan), SEM-EDX (Hitachi SU8020, Tokyo, Japan/Jeol JSM-IT200, Tokyo, Japan), and XRD Siemens D5000 (Munich, Germany) with a cobalt anticathode ($\lambda = 1.78 \text{ \AA}$) and Panalytical (Malvern Panalytical Ltd., UK) with a copper anticathode ($\lambda = 1.54 \text{ \AA}$) to identify the crystalline phases. The Rietveld analysis was performed using Profex 5.5.0, an open-access software.

Samples were tested for hardness by the Vickers method using a 30 kg load with an EMCO-TEST, (Kuchl, Austria) instrument. The toughness was calculated by the Palmqvist method [14].

The medium grain size for a sample was calculated as the figure's surface divided by the number of grains manually counted, inspired by ASTM E112 [15]. For this purpose, high-magnification SEM images (10,000 \times) were used.

3. Results and Discussion

The powders fabricated by wet milling with different kinds of balls were analyzed by X-ray diffraction (Figure 1).

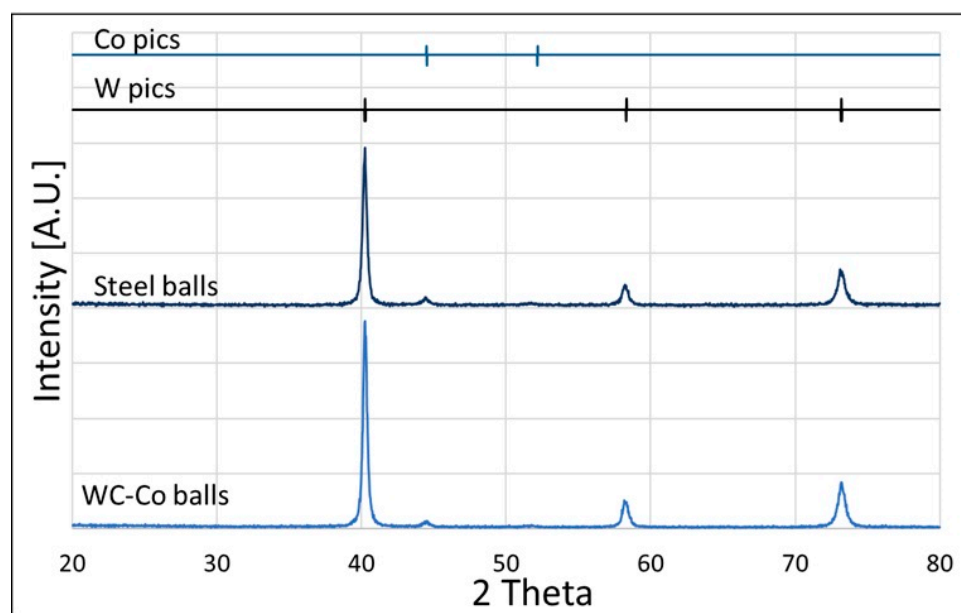


Figure 1. XRD patterns for W-C powder mixture after 10 h of milling. Only peaks corresponding to tungsten and cobalt are present.

Due to the amorphous nature of black carbon, only the peaks of tungsten and cobalt are visible. Cobalt exists in the FCC form (peaks at 44.5° and 52.15°), but its intensity is low compared to that of tungsten. Additionally, no signs of contamination were detected by the XRD analysis, although minor contamination with iron from milling ball wear is quite probable. In both batches of milled powder, there were no significant contaminations from iron or tungsten carbide resulting from the wear of milling tools. Furthermore, as

demonstrated in a previous study, milling parameters do not provide enough energy to initiate carburization during milling and homogenization [16].

The XRD pattern of the sintered samples is shown in Figures 2 and 3. The Rietveld analysis was carried out using the Profex 5.5.0 software. The XRD diffractograms with the Rietveld analysis are displayed in Figure 3 for the samples ground with steel tools and in Figure 4 for the samples milled with WC-6Co tools. The proportion of detected phases is listed in Table 2. The WC peaks are prominent, while the cobalt peaks are very small. The tungsten peaks are no longer visible in the diffractogram, indicating that the tungsten has been completely converted into tungsten carbide. Several cobalt-containing phases were identified, most of which were at the detection limit. Chromium carbide was not detected in the WC-6Co ball-milled mixture and was at the detection limit in the steel ball-milled samples, suggesting that the prior homogenization with cobalt effectively achieved a homogeneous distribution of the grain growth inhibitor. The eta phase (an undesirable, fragile carbide of the M_6C or $M_{12}C$ type, which occurs due to a local lack of carbon) appears in very small quantities, especially in samples milled with steel balls. The $M_{12}C$ form (W_6Co_6C) is present in larger amounts in the steel ball-milled sample but does not exceed 2 wt.%.

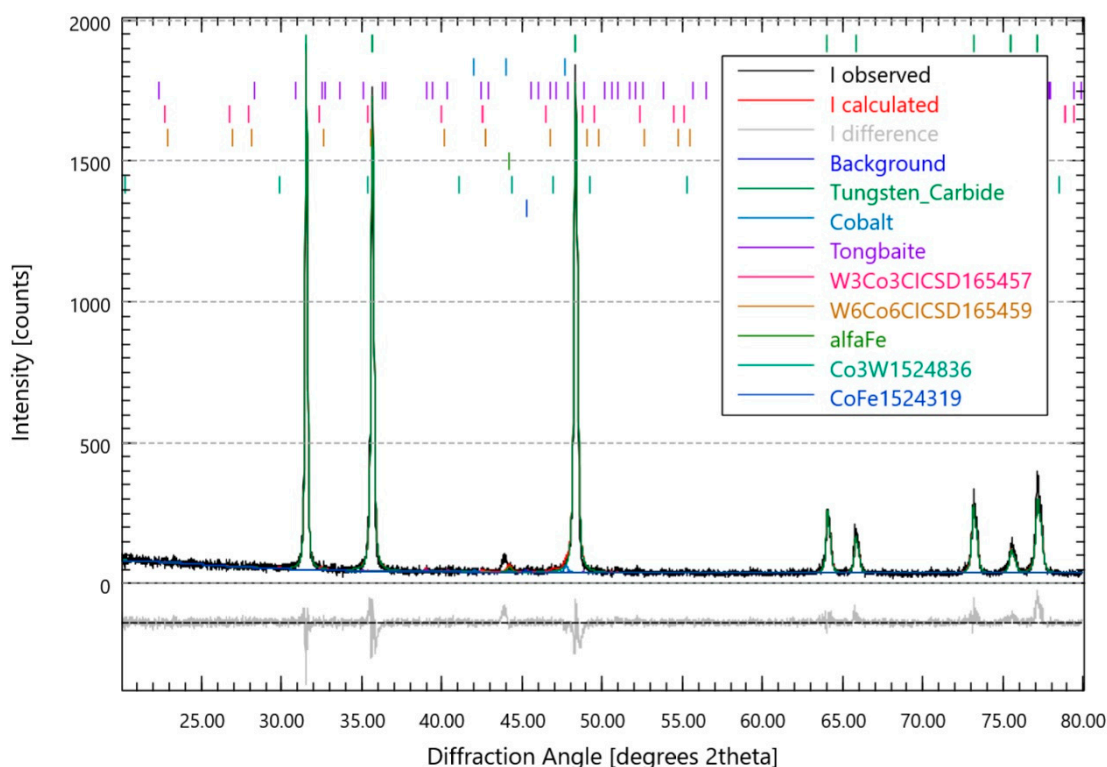


Figure 2. XRD pattern and Rietveld refinement for samples milled with steel balls.

Table 2. Phase proportion after Rietveld refinement.

Phase	Phase Proportion	
	Milled with Steel Balls	Milled with WC-6Co Balls
Qwc	0.91 ± 0.05	0.97 ± 0.02
QCobalt	0.02 ± 0.02	0.02 ± 0.02
QTongbaite Cr ₃ C ₂	0.02 ± 0.04	0 ± 0
QW ₃ Co ₃ C	0.006 ± 0.009	0.001 ± 0.004
QW ₆ Co ₆ C	0.014 ± 0.009	0 ± 0.004
Q alfaFe	0.017 ± 0.01	0.003 ± 0.009
QCo ₃ W	0.004 ± 0.01	0.003 ± 0.007
QCoFe	0.007 ± 0.01	0 ± 0

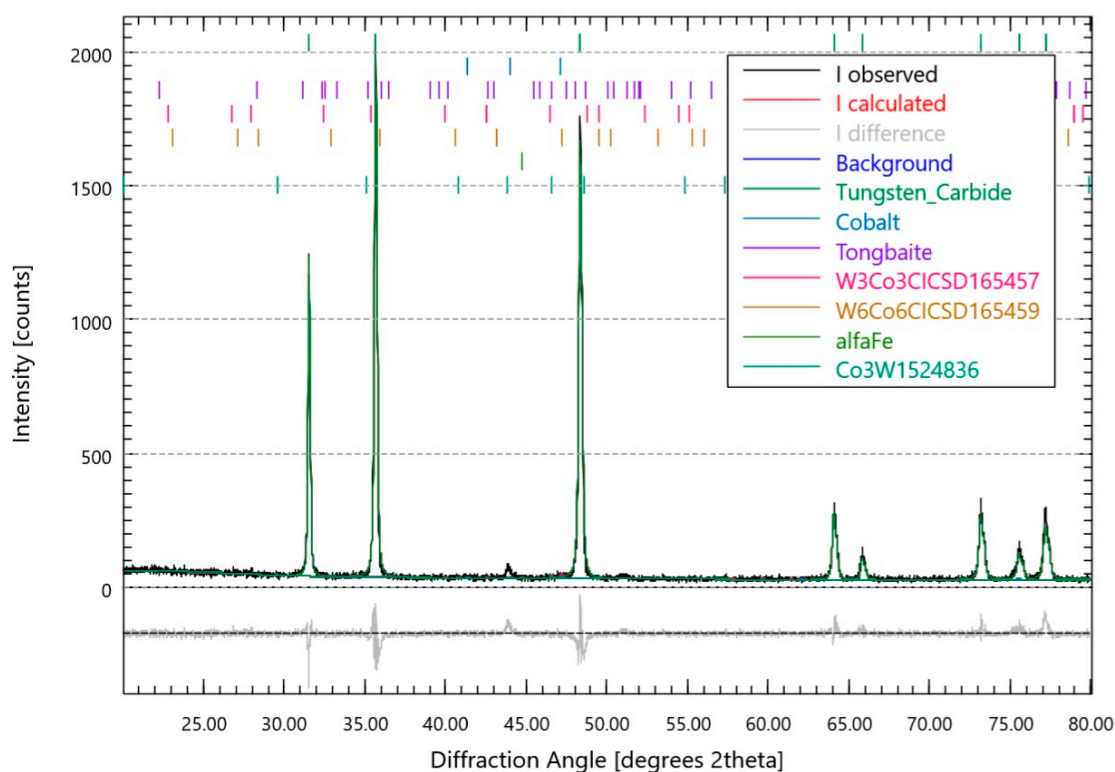


Figure 3. XRD pattern and Rietveld refinement for samples milled with WC-6Co balls.

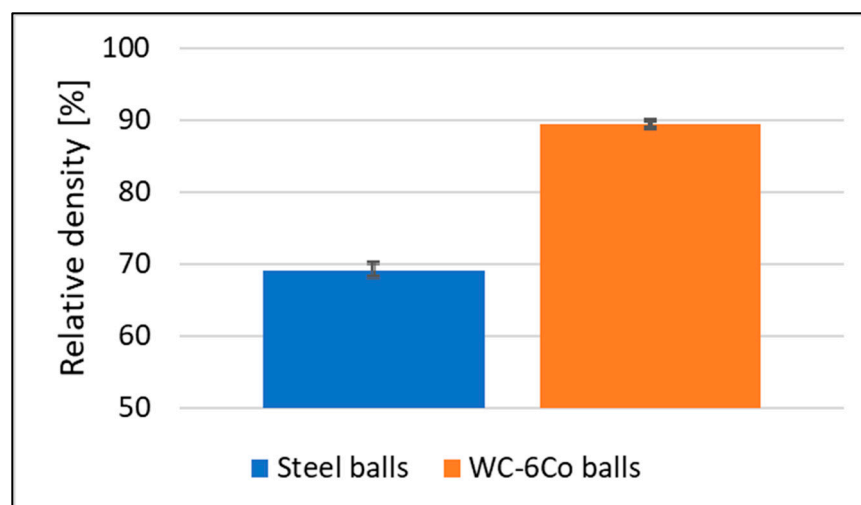


Figure 4. Sample density measured by Archimedes' principle.

This is caused by oxygen absorption on the surface during milling, which is reduced by carbon from the carbides, leading to the formation of the eta phase. To prevent this, it is recommended to use a sintering atmosphere with a higher redox potential [17,18].

The presence of the eta phase was also reported by Wangbin Zhan [6] when the reaction occurs above 1100 °C. To avoid the appearance of this phase, he recommends maintaining the temperature constant at 850 °C until carburization is complete. However, this process takes a very long time; in his study, after 10 h at 850 °C, only 50% of the tungsten was transformed into WC.

Iron is also present in higher proportions in milled steel tool samples, which is normal.

Although the proportion of cobalt is lower than the actual amount, it must be acknowledged that phases containing elements with a high atomic number absorb more

radiation than those with lighter elements. In a quantitative analysis, these phases tend to be overestimated [19].

The density of the samples was measured using Archimedes' method. The results are shown in Figure 4. Samples milled with WC-Co balls have a significantly higher density than those milled with steel balls. The densification of powders milled with WC-Co balls reaches nearly 90%, whereas for the samples made with steel-milled powder, it is about 70%.

This difference can be attributed to the higher reactivity of the powder, which is caused by the increased energy generated during milling by the heavier balls [16]. Of course, these values fall below the requirements for industrial applications (+99%), and solutions such as pressure-assisted sintering (sinterHIP) can make up for this shortfall [20]. In any case, the study will continue to optimize other parameters, such as the pressing force and sintering temperature, to overcome this drawback and ensure densities close to the theoretical level.

To examine the samples' microstructure, several specimens were sectioned based on their diameter, mounted in resin, and polished. A cross-sectional view of the samples is shown in Figure 5. Figure 5a,b reveal that concave cracks connect the corners of the samples. These cracks form due to internal stress within the sample, induced during powder compaction [21–25]. Pressure is unevenly distributed throughout the powder due to friction with the mold wall and the piston's surface, creating regions of different densities and varying internal stresses, which lead to cracking [26]. In this case, the most probable cause is the use of a manual hydraulic press, which does not allow uniform pressure application during sample pressing. Another source of internal defects is the inability to expel gases produced during sintering by reducing the oxides inherently present on the surface of the particles [17].

The presence of these voids in the samples' structure explains the low density recorded and favors the additional cracking of the samples during the cutting.

To avoid this situation, it is essential to control the powder homogeneity and chemical composition more rigorously during sintering to prevent the formation of the eta phase, which induces fragility [27]. The absence of carbon results in a higher dissolution of tungsten into cobalt, the appearance of more liquid phases, and an increased eta phase during solidification [28]. Problems caused by uneven pressing can be fixed by using a press that maintains consistent pressure (such as bilateral pressing) and/or by employing a pressure-assisted sintering method, like SinterHIP, which significantly reduces porosity by applying pressure during the hold period at the sintering temperature [29,30].

The delamination of the samples perpendicular to the pressing direction reveals several "levels" where the material is dense. Few porosities are observed, mostly small in size, around one micron, and, more rarely, pores ranging from 10 to 30 μm (Figure 5c,d). The SEM investigation results are shown in Figures 6 and 7. Low residual porosity is noted, with pore sizes of 1 to 2 microns.

The tungsten carbide grains are well individualized, exhibiting a characteristic prismatic shape for this material [31]. The grain size is relatively uniform, with no evident abnormal grain growth (AGG), thanks to a good distribution of the grain growth inhibitor (GGI), achieved not through prolonged milling of the mixture but by utilizing a doped binder [32]. The average grain size for samples milled with steel balls (Figure 6b) is 0.70 μm , while for samples milled with WC-6Co balls (Figure 6d), it is 0.32 μm . The detailed microstructure of the samples milled with WC-6Co balls is shown in Figure 7. The WC grain size does not exceed 3 μm , and many submicronic grains are visible. The average grain size for Figure 7 is 0.32 μm , calculated as the figure's surface divided by the manually counted number of grains.

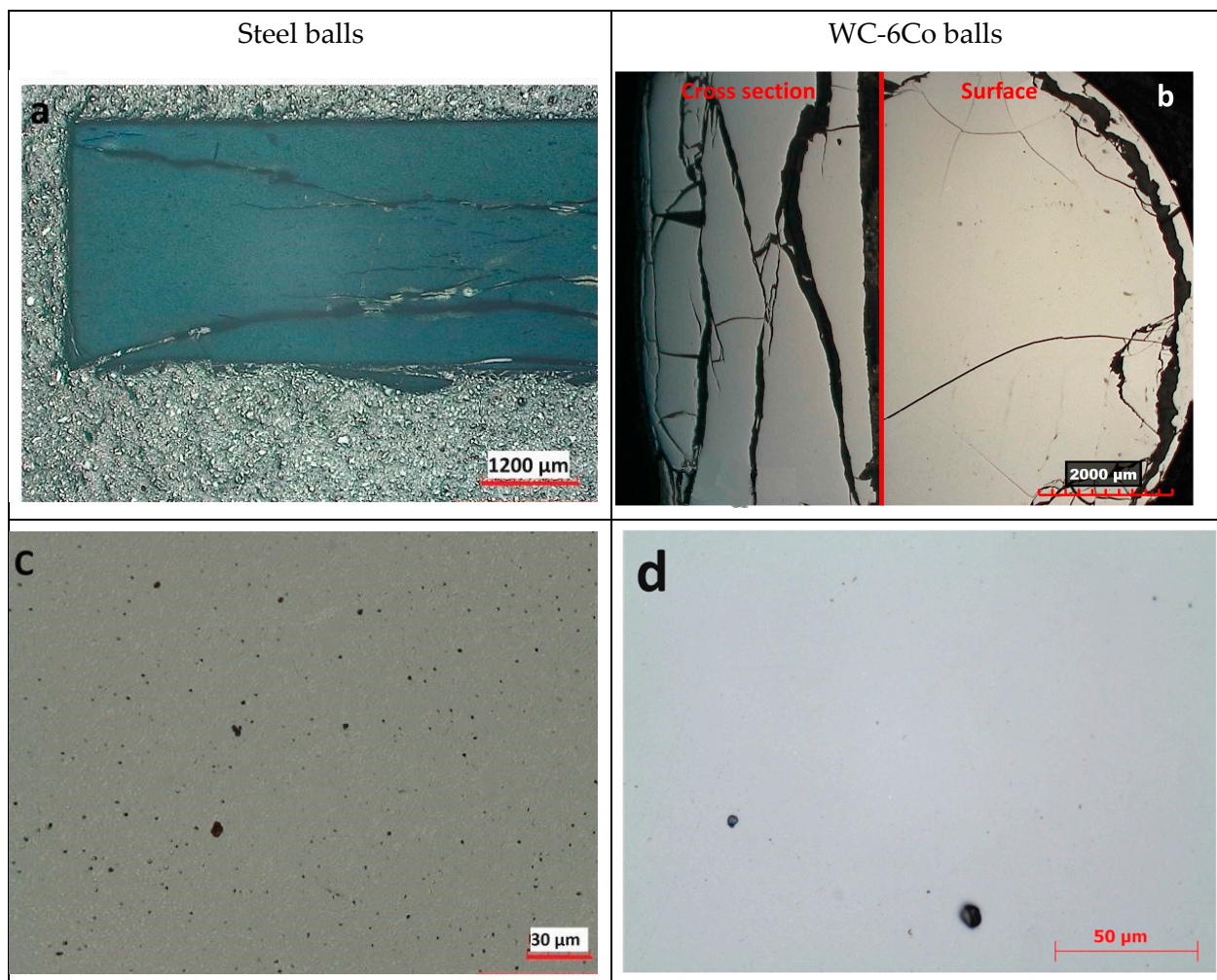


Figure 5. Samples' macrostructure after cutting and mounting in resin ((a,b) MO 35 \times , no etching), and details of the dense zones ((c,d) OM, 1000 \times , no etching).

The chemical composition of the samples, measured by EDS, is presented in Table 3. Although this method of determining chemical composition is not very precise for carbon (due to the presence of oil vapors from the vacuum pump), the results are very close to the nominal composition of this material: 84.5 wt.% W, 5.517 wt.% C, 9 wt.% Co, and 1 wt.% Cr₃C₂.

Table 3. Chemical composition of sintered samples (Figure 4).

	Chemical Composition [% , by Weight]				
	C	Cr	Fe	Co	W
<i>Steel balls</i>	5.80	1.02	1.320	8.75	83.10
<i>WC balls</i>	5.38	0.77		9.32	84.7

Contamination with iron from the milling media is also observed. This wear explains the higher chromium content in the samples milled with steel balls, as these milling media contain a high chromium content. Weak detection of iron by X-ray diffraction in the samples milled with WC-6Co occurred, because it is present in small quantities and is dissolved in other phases. Traditionally, the presence of iron in the binder composition was avoided, because iron has lower oxidation resistance than cobalt, especially at high temperatures during milling or turning [33]. However, the use of iron as a binder has been pursued for 50 years, driven by research led by Leo Prakash [34,35]. In recent years, many studies have

been conducted to replace cobalt with various iron-based alloys [36–43]. The properties of composites with alternative binders are inferior to those with cobalt binders [44–47], although some of them are better [48]. Nevertheless, the presence of iron along with certain other elements does not negatively impact the behavior of such materials [40].

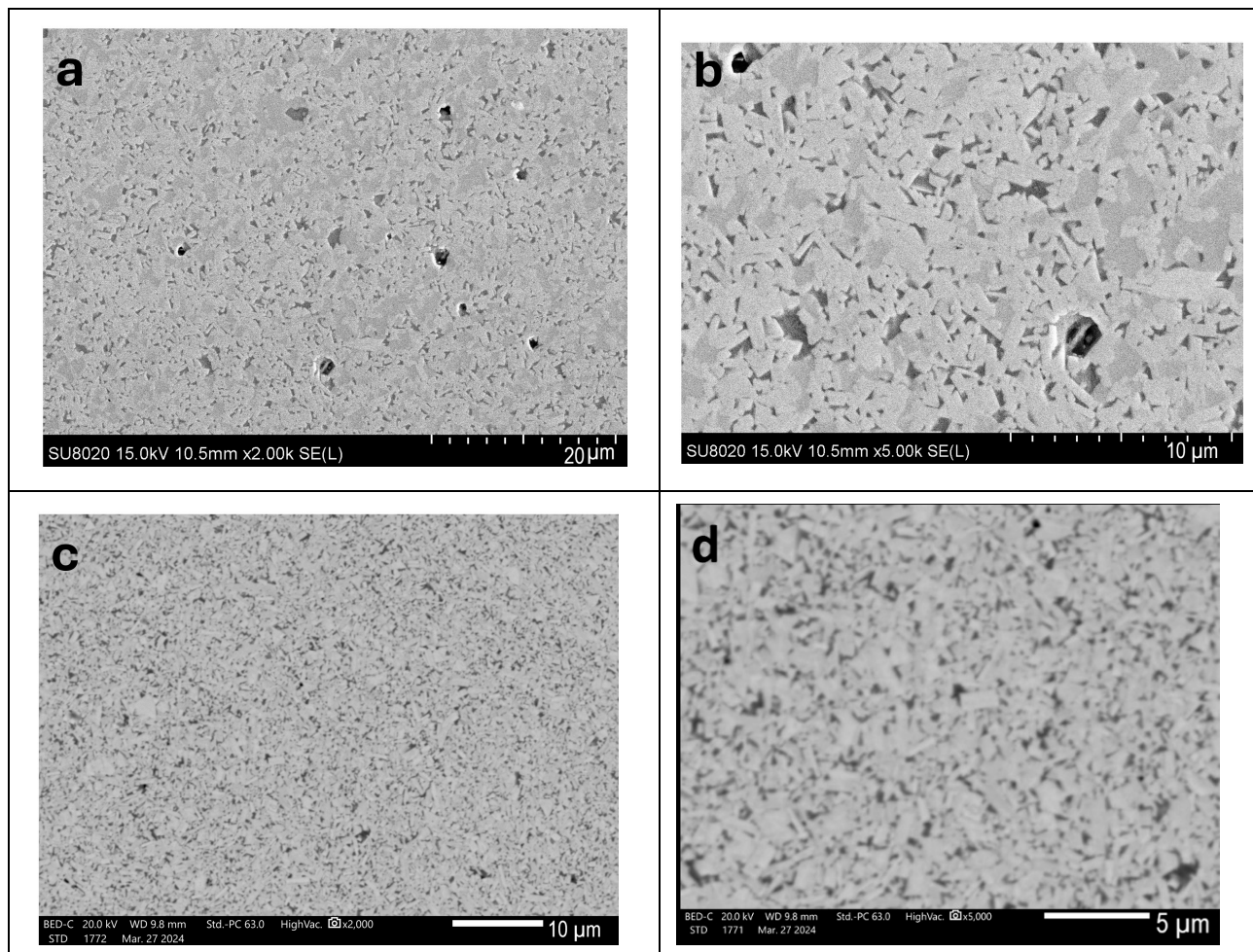


Figure 6. Microstructure of sintered samples: (a,b) samples milled with steel balls; (c,d) samples milled with WC-Co balls. SEM at 2000 \times and 5000 \times , respectively.

From the perspective of mechanical properties, the samples were tested for hardness using the Vickers method with a 30 kg load. The results are presented in Table 4. Samples made with powder milled using WC-Co balls exhibit slightly higher hardness values (1809 HV30) compared to 1762 HV30 for the steel ball-milled samples. This is attributed to a more homogeneous microstructure. One explanation for this is that a greater amount of energy is transferred to the powder during milling, as WC-Co balls are twice as heavy as steel balls [16].

The obtained hardness is very good, with values in the upper range of typical results (1000–1900 HV) for this type of composition [14]. The toughness results are also quite satisfactory, as literature data collected by A. Chychko and others [14] show toughness values between 9 and 11 MPa·m^{1/2} for WC-9 wt.% Co compositions with a density above 98%. Porosity does not appear to have a major impact on hardness but does significantly reduce toughness [49]. We expect that improving the density will lead to a noticeable increase in toughness.

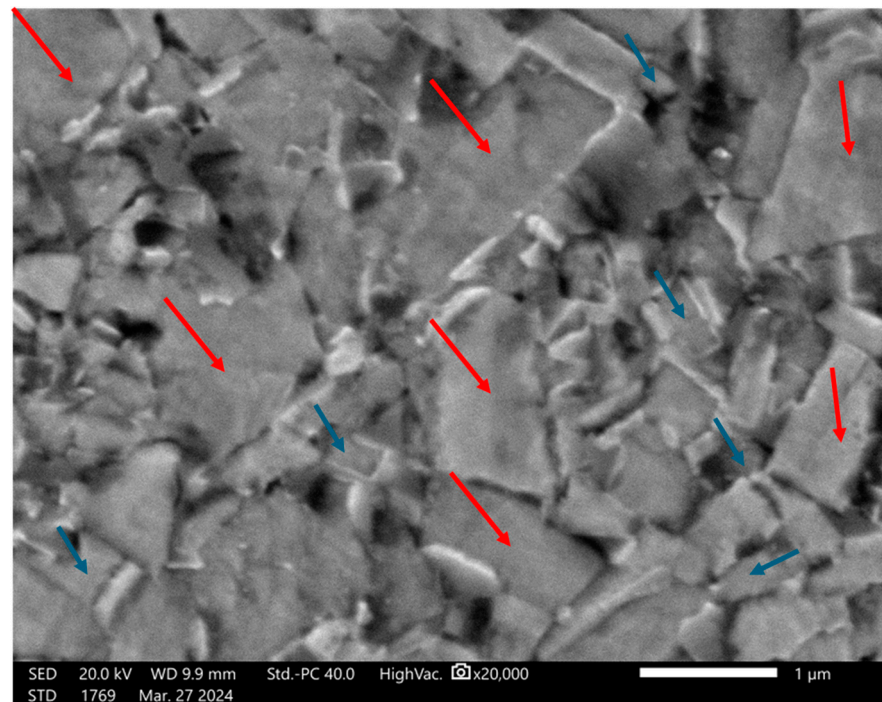


Figure 7. Microstructure of samples milled with WC-Co balls after sintering. SEM, in SE mode, at 20,000 \times (blue arrows indicate the smallest grains, or micrograins, and the red ones, the biggest ones).

Table 4. Mechanical properties for sintered samples.

	Hardness [HV30]		Toughness [MPa \times m ^{1/2}]	
	Steel balls	WC-Co balls	Steel balls	WC-Co balls
Value	1762	1809	10.81	10.98
Standard deviation	22.3	61.0	1.6	1.2

4. Conclusions

The purpose of this study was to examine the reliability of producing WC-Co parts using elemental powders, tungsten carburization, and the sintering of parts developed during the same thermal cycle.

After analyzing the results obtained, we can say the following:

The reactive sintering of tungsten, carbon, and cobalt powders was successfully conducted in normal sintering conditions for WC-Co composites.

The obtained product has good mechanical properties, with a hardness of 1800 HV30.

The toughness of samples reaches a value of 10.9 MPa \times m^{1/2}. This value falls within the range reported in the literature and can be increased by enhancing the density.

A small amount of the fragile eta phase is present in the samples' microstructure: better control of the carbon balance is thus necessary. The absence of the eta phase will improve toughness.

It is necessary to optimize the homogenization process of the powder to prevent segregation and the formation of cracks when extracting from the mold, which increases green strength, as is the case when using bilateral pressing.

The use of WC-6Co balls (twice as heavy steel balls) ensures better densification due to a higher degree of powder activation, which provides better reactivity during sintering.

Densification is not satisfactory at this stage of research. Pressure-assisted sintering will be necessary to achieve densities close to 100%.

In conclusion, it is perfectly possible to produce WC-Co composites by reactive sintering of elementary powders with properties necessary for wear tools.

From this perspective, it will be necessary to optimize pressing and sintering in terms of temperature to improve density towards values suitable for industry applications.

Author Contributions: Conceptualization, V.I.S. and F.D.; methodology, V.I.S.; validation, V.I.S., V.V. and F.D.; formal analysis, V.I.S., A.M. (Alexandre Mégret) and A.M. (Anne Mouftiez); investigation, V.I.S., A.M. (Alexandre Mégret) and A.M. (Anne Mouftiez); resources, V.I.S.; data curation, V.I.S.; writing—original draft preparation, V.I.S.; writing—review and editing, F.D. and V.I.S.; visualization, V.V. and F.D.; supervision, F.D.; project administration, V.I.S.; funding acquisition, F.D. All authors have read and agreed to the published version of the manuscript.

Funding: This research received no external funding.

Data Availability Statement: The raw data supporting the conclusions of this article will be made available by the authors on request.

Acknowledgments: The authors gratefully acknowledge the research center Materia Nova for analyses by electron microscopy.

Conflicts of Interest: The authors declare no conflict of interest.

References

1. Schwartzkopf, P.; Richard, K. *Cemented Carbides*; The Macmillan Company: New York, NY, USA, 1960.
2. Wolfe, P.K.; Johnson, T.A.; Mehrota, J.L. Production of Carbide Powders. In *ASM Handbook, Volume 7, Powder Metallurgy*; ASM International: Almere, the Netherlands, 2015; pp. 711–714. Available online: <https://matdata.asminternational.org/hbk/> (accessed on 2 March 2025).
3. Mühlbauer, G.; Kremser, G.; Bock, A.; Weidow, J.; Schubert, W.-D. Transition of W₂C to WC during carburization of tungsten metal powder. *Int. J. Refract. Met. Hard Mater.* **2018**, *72*, 141–148. [CrossRef]
4. Seegopaul, P.; McCandlish, L.; Shinneman, F. Production capability and powder processing methods for nanostructured WC-Co powder. *Int. J. Refract. Met. Hard Mater.* **1997**, *15*, 133–138. [CrossRef]
5. Luković, J.; Babić, B.; Bučevac, D.; Prekajski, M.; Pantić, J.; Baščarević, Z.; Matović, B. Synthesis and characterization of tungsten carbide fine powders. *Ceram. Int.* **2015**, *41*, 1271–1277. [CrossRef]
6. Zhan, W.; Wang, H.; Liang, S.; Liu, X.; Song, X. Acceleration effect of cobalt on carburization of tungsten at low temperature. *J. Alloy. Compd.* **2018**, *732*, 429–435. [CrossRef]
7. Popov, O.; Vishnyakov, V. High Densification of Tungsten via Hot Pressing at 1300 °C in Carbon Presence. *Materials* **2022**, *15*, 3641. [CrossRef] [PubMed]
8. Calabrese, M.; Portarapillo, M.; Di Nardo, A.; Venezia, V.; Turco, M.; Luciani, G.; Di Benedetto, A. Hydrogen Safety Challenges: A Comprehensive Review on Production, Storage, Transport, Utilization, and CFD-Based Consequence and Risk Assessment. *Energies* **2024**, *17*, 1350. [CrossRef]
9. Sun, S.-K.; Zhang, G.-J.; Wu, W.-W.; Liu, J.-X.; Zou, J.; Suzuki, T.; Sakka, Y. Reactive spark plasma sintering of binderless WC ceramics at 1500 °C. *Int. J. Refract. Met. Hard Mater.* **2014**, *43*, 42–45. [CrossRef]
10. Sun, S.; Kan, Y.; Zhang, G.; Dariel, M.P. Fabrication of Nanosized Tungsten Carbide Ceramics by Reactive Spark Plasma Sintering. *J. Am. Ceram. Soc.* **2011**, *94*, 3230–3233. [CrossRef]
11. Aouchiche, L.; Alhussein, A.; Nechiche, M.; Retraint, D.; Amirouche, S.; Azem, S. Microstructural, mechanical and tribological characterization of Co–20 wt% WC composite elaborated by solid-phase sintering of Co–W–C powders mixture. *Tribol. Mater. Surfaces Interfaces* **2021**, *16*, 202–210. [CrossRef]
12. Stanciu, V.I.; Vitry, V.; Delaunois, F. Cobalt-inhibitor mixtures for cemented carbides. In Proceedings of the 19th Plansee Semin, Reutte, Austria, 29 May–2 June 2017; Volume 2017, pp. 1–13.
13. Sadangi, R.; Bose, A. Some aspects of solid solution grain growth inhibitors in cemented tungsten carbides. *Int. J. Refract. Met. Hard Mater.* **2024**, *119*, 106474. [CrossRef]
14. Chychko, A.; García, J.; Ciprés, V.C.; Holmström, E.; Blomqvist, A. HV-KIC property charts of cemented carbides: A comprehensive data collection. *Int. J. Refract. Met. Hard Mater.* **2022**, *103*, 105763. [CrossRef]

15. ASTM E112-24; Standard Test Methods for Determining Average Grain Size. ASTM International: Almere, The Netherlands, 2024. Available online: <https://store.astm.org/e0112-24.html> (accessed on 12 July 2025).
16. Stanciu, V.I.; Vitry, V.; Delaunois, F. Study of the milling parameters optimization in the direct carburization of WO₃ by mechanical alloying. *Int. J. Refract. Met. Hard Mater.* **2020**, *87*, 105160. [\[CrossRef\]](#)
17. Bose, A.; Sadangi, R.; Mehrotra, P.K. Sintering of Hardmetals. In *ASM Metallurgy Handbook Vol. 7—Powder Metallurgy*; ASM Handbook; ASM International: Almere, The Netherlands, 2018; pp. 720–725. [\[CrossRef\]](#)
18. Parker, S.; Whiting, M.; Yeomans, J. Control of carbon content in WC-Co hardmetal by heat treatment in reducing atmospheres containing methane. *Int. J. Refract. Met. Hard Mater.* **2017**, *66*, 204–210. [\[CrossRef\]](#)
19. Pederson, B.M.; Gonzalez, R.M.; Winburn, R.S. Minimization of microabsorption effects in complex mixtures. *Adv. X-Ray Anal.* **2003**, *46*, 68–73.
20. Shi, X.; Shao, G.; Duan, X.; Xiong, Z.; Yang, H. Characterizations of WC–10Co nanocomposite powders and subsequently sinterhip sintered cemented carbide. *Mater. Charact.* **2006**, *57*, 358–370. [\[CrossRef\]](#)
21. Long, W.M. Radial Pressures in Powder Compaction. *Powder Metall.* **1960**, *3*, 73–86. [\[CrossRef\]](#)
22. Rödiger, K.; Berg, H.v.D.; Dreyer, K.; Kassel, D.; Orth, S. Near-net-shaping in the hardmetal industry. *Int. J. Refract. Met. Hard Mater.* **2000**, *18*, 111–120. [\[CrossRef\]](#)
23. James, W.B.; Retired, H.C. Nondestructive Evaluation of Pressed and Sintered Powder Metallurgy Parts. *Nondestruct. Eval. Mater.* **2018**, *17*, 533–543. [\[CrossRef\]](#)
24. Galen, S.; Zavaliangos, A. Strength anisotropy in cold compacted ductile and brittle powders. *Acta Mater.* **2005**, *53*, 4801–4815. [\[CrossRef\]](#)
25. Uematsu, K. Processing defects in ceramic powders and powder compacts. *Adv. Powder Technol.* **2014**, *25*, 154–162. [\[CrossRef\]](#)
26. Tatarinov, A.; Kurtenoks, V.; Mironovs, V. Detection of cracks in green products of powder metallurgy by means of laser vibrometry. In *Proceedings of the Modern Materials and Manufacturing (MMM 2021), Tallinn, Estonia, 27–29 April 2021*; IOP Conference Series: Materials Science and Engineering; IOP Publishing Ltd.: Bristol, UK, 2021; Volume 1140, p. 012045. [\[CrossRef\]](#)
27. Schade, C. Blending and Premixing of Metal Powders and Binders. *Powder Metall.* **2018**, *7*, 88–92. [\[CrossRef\]](#)
28. Konyashin, I.; Zaitsev, A.; Sidorenko, D.; Levashov, E.; Ries, B.; Konishev, S.; Sorokin, M.; Mazilkin, A.; Herrmann, M.; Kaiser, A. Wettability of tungsten carbide by liquid binders in WC–Co cemented carbides: Is it complete for all carbon contents? *Int. J. Refract. Met. Hard Mater.* **2017**, *62*, 134–148. [\[CrossRef\]](#)
29. Fabijanić, T.A.; Alar, Ž.; Ćorić, D. Influence of consolidation process and sintering temperature on microstructure and mechanical properties of near nano- and nano-structured WC-Co cemented carbides. *Int. J. Refract. Met. Hard Mater.* **2016**, *54*, 82–89. [\[CrossRef\]](#)
30. Schwarz, V.; Shi, K.; Lengauer, W. Metallurgy and Properties of Mo-doped WC-Co and (W,Mo)C-Co Hardmetals. In *Proceedings of the WorldPM 2016, Hamburg, Germany, 9–13 October 2016*.
31. Kumar, V.; Fang, Z.Z.; Wright, S.I.; Nowell, M.M. An analysis of grain boundaries and grain growth in cemented tungsten carbide using orientation imaging microscopy. *Met. Mater. Trans. A* **2006**, *37*, 599–607. [\[CrossRef\]](#)
32. Stanciu, V.I.; Erauw, J.-P.; Boilet, L.; Vitry, V.; Delaunois, F. WC-Co composite made with doped binder: The effect of binder proportion on microstructure and mechanical properties. *Int. J. Refract. Met. Hard Mater.* **2023**, *112*, 106161. [\[CrossRef\]](#)
33. Toller, L.R.M.; Norgren, S.M. Mechanisms of plastic deformation in WC-Co and WC-Ni-Fe turning inserts. In *Proceedings of the 19th Plansee Seminar, Reutte, Austria, 29 May–2 June 2017*.
34. Prakash, L.J. Development of Tungsten Carbide Hardmetals Using Iron-Based Binder Alloys. Ph.D. Thesis, Inst. fuer Material- und Festkoerperforschung, Fakultät fuer Maschinenbau, Karlsruhe University, Karlsruhe, Germany, 1980. Available online: <https://inis.iaea.org/records/k0pd9-fjt74> (accessed on 12 July 2025).
35. Prakash, L.J. Properties and applications of WC hardmetals with iron based binders. In *Proceedings of the Ninth International Conference on Tungsten, Refractory & Hardmaterials, Orlando, FL, USA, 18–22 May 2014*; pp. 113–125.
36. Humphry-Baker, S.A.; Marshall, J.M.; Smith, G.D.W.; Lee, W.E. Thermophysical properties of Co-free WC-FeCr hardmetals. In *Proceedings of the 19th Plansee Seminar, Reutte, Austria, 29 May–2 June 2017*.
37. Fang, Z.Z.; Wang, X.; Ryu, T.; Hwang, K.S.; Sohn, H. Synthesis, sintering, and mechanical properties of nanocrystalline cemented tungsten carbide—A review. *Int. J. Refract. Met. Hard Mater.* **2009**, *27*, 288–299. [\[CrossRef\]](#)
38. Linder, D.; Holmström, E.; Norgren, S. High entropy alloy binders in gradient sintered hardmetal. In *Proceedings of the 19th Plansee Seminar, Reutte, Austria, 29 May–2 June 2017*; pp. 1–7.
39. Alvaredo, P.; Cornide, J.; Prieto, E.; Gordo, M.N.E. High Entropy Alloy as Binder in Cermets. In *Proceedings of the Euro PM 2018 Congress and Exhibition, Bilbao, Spain, 14–18 October 2018*.
40. de Nicolás-Morillas, M.; Besharatloo, H.; Cabezas, L.; de la Mata, M.; Sales, D.; Pereira, L.; Müller-Grunz, A.; Bertalan, C.; Useldinger, R.; Llanes, L.; et al. Processing of WC with Fe-based alternative binders: Adjustment of C content and effect of Cr addition. *Int. J. Refract. Met. Hard Mater.* **2024**, *118*, 106444. [\[CrossRef\]](#)

41. Rosa, J.M.B.; Lugon, R.D.; Silva, K.d.S.; das Chagas, V.M.; Guimarães, R.d.S.; de Carvalho, C.S.; Barreto, L.P.d.P.; Filgueira, M. Study of characteristics and properties of spark plasma sintered WC with the use of alternative Fe-Ni-Nb binder as Co replacement. *Int. J. Refract. Met. Hard Mater.* **2020**, *92*, 105316. [[CrossRef](#)]
42. Schubert, W.; Fugger, M.; Wittmann, B.; Useldinger, R. Aspects of sintering of cemented carbides with Fe-based binders. *Int. J. Refract. Met. Hard Mater.* **2015**, *49*, 110–123. [[CrossRef](#)]
43. Soria-Biurrun, T.; Lozada-Cabezas, L.; Ibarreta-Lopez, F.; Martinez-Pampliega, R.; Sanchez-Moreno, J. Effect of chromium and carbon contents on the sintering of WC-Fe-Ni-Co-Cr multicomponent alloys. *Int. J. Refract. Met. Hard Mater.* **2020**, *92*, 105317. [[CrossRef](#)]
44. Toller, L.; Norgren, S. Phase Transformations in Iron-Based Alternative Binders for Hardmetals. In Proceedings of the 2016 Powder Metallurgy World Congress, Hamburg, Germany, 9–13 October 2016; EPMA, Ed.; EPMA: Hambourg, Germany, 2016.
45. Sáez, I.; Torralba, J.M. Novel WC Hardmetal with Cr/Fe Binder Alloy Sintered by SPS. In Proceedings of the 2016 Powder Metallurgy World Congress, Hamburg, Germany, 9–13 October 2016; EPMA, Ed.; EPMA: Hambourg, Germany, 2016; pp. 1–5.
46. Roulon, Z.; Missiaen, J.-M.; Lay, S. Effect of Binder Phase on Sintering of Cemented Carbides. In Proceedings of the 2018 Powder Metallurgy World Congress, Beijing, China, 16–20 September 2018; pp. 770–774.
47. Buchegger, C.; Lengauer, W.; Bernardi, J.; Gruber, J.; Ntaflos, T.; Kiraly, F.; Langlade, J. Diffusion parameters of grain-growth inhibitors in WC based hardmetals with Co, Fe/Ni and Fe/Co/Ni binder alloys. *Int. J. Refract. Met. Hard Mater.* **2015**, *49*, 67–74. [[CrossRef](#)]
48. Nakonechnyi, S.; Yurkova, A.; Loboda, P. WC-based cemented carbide with NiFeCrWMo high-entropy alloy binder as an alternative to cobalt. *Vacuum* **2024**, *222*, 113052. [[CrossRef](#)]
49. Chen, C.; Huang, B.; Liu, Z.; Chen, L.; Li, Y.; Zou, D.; Chang, Y.; Cheng, X.; Zhou, R.; Liu, Y. Material extrusion additive manufacturing of WC-9Co cemented carbide. *Addit. Manuf.* **2024**, *86*, 104203. [[CrossRef](#)]

Disclaimer/Publisher’s Note: The statements, opinions and data contained in all publications are solely those of the individual author(s) and contributor(s) and not of MDPI and/or the editor(s). MDPI and/or the editor(s) disclaim responsibility for any injury to people or property resulting from any ideas, methods, instructions or products referred to in the content.